Preclinical Evaluation of a High-Affinity ^{18}F-Trifluoroborate Octreotate Derivative for Somatostatin Receptor Imaging

Zhibo Liu*[1], Maral Pourghiasian*[2], François Bénard[2], Jinhe Pan[2], Kuo-Shyan Lin[2], and David M. Perrin[1]

[1]Chemistry Department, University of British Columbia, Vancouver, British Columbia, Canada; and [2]BC Cancer Agency Research Centre, Vancouver, British Columbia, Canada

Recent studies have highlighted the high sensitivity of PET imaging with ^{68}Ga-labeled octreotide derivatives for the detection and staging of neuroendocrine tumors. A somatostatin receptor ligand that is easily radiolabeled with ^{18}F-fluoride could improve the availability of PET imaging of neuroendocrine tumors. We report an alkyltrifluoroborate–octreotate conjugate that is radiolabeled in a 1-step ^{18}F exchange reaction in high yield and with high specific activity. **Methods:** We conjugated a new alkyltrifluoroborate to octreotate to obtain AMBF$_3$-TATE, which was stored in 50-nmol aliquots for radiolabeling. [18]F labeling was performed by [18]F-^{19}F isotope exchange with ^{18}F-fluoride, and the tracer was purified by C18 cartridge separation. The radiochemical yield was 20%–25%. PET imaging and biodistribution were performed on mice bearing AR42J tumor xenografts. **Results:** AMBF$_3$-TATE bound the somatostatin receptor subtype 2 with high affinity (inhibition constant, 0.13 ± 0.03 nM). Starting with 29.6–37 GBq (0.8–1 Ci) of ^{18}F-fluoride, more than 7.4 GBq (>200 mCi) of ^{18}F-AMBF$_3$-TATE were obtained in 25 min ($n = 5$) with greater than 99% radiochemical purity at high specific activity (>111 GBq [3 Ci]/µmol). ^{18}F-AMBF$_3$-TATE was stable in plasma. PET imaging and biodistribution showed rapid renal excretion with low liver activity. High tumor uptake (10.11% ± 1.67% injected dose/g, $n = 5$) was detected at 60 min after injection. Bone uptake was negligible. Tumor-to-liver, tumor-to-blood, tumor-to-muscle, and tumor-to-bone ratios (at 60 min) were 26.2 ± 0.8, 25.1 ± 1.0, 89.0 ± 3.1, and 21.3 ± 3.6, respectively. **Conclusion:** ^{18}F-AMBF$_3$-TATE was radiolabeled in high yield and at high specific activity, did not require high-performance liquid chromatography purification, exhibited unexpectedly high binding affinity to somatostatin receptor subtype 2, and showed excellent pharmacokinetic properties in vivo, with high tumor uptake and high contrast ratios.

Key Words: positron emission tomography; somatostatin receptor; octreotide; octreotate; ^{18}F-BF$_3$; 1-step ^{18}F-labeling

The somatostatin receptor subtype 2 (sstr2) is overexpressed in many neuroendocrine tumors. Hence, over the past 30 y there

has been considerable interest in developing high-affinity somatostatin-derived ligands that bind sstr2, notably for radionuclide therapy (*1*). To diagnose and monitor patients with sstr2-positive tumors, radiotracers based on the somatostatin family of peptides (*2–5*), notably octreotate (TATE) and octreotide, have been labeled with various radioisotopes for noninvasive imaging. ^{111}In-diethyle-netriaminepentaacetic acid-pentetreotide (Octreoscan; Mallinckrodt) is the current clinical standard for imaging neuroendocrine tumors (*6–8*). [99m]Tc derivatives such as ^{99m}Tc-depreotide (*9*) and ^{99m}Tc-hydrazinonicotinyl-Tyr[3]-octreotide have also been used (*10*) but are not commercialized in North America.

For PET imaging, ^{68}Ga, ^{64}Cu, and ^{18}F along with various radioprosthetics have been conjugated to various octreotide derivatives (*11–16*). Of these, certain ^{68}Ga ligands such as ^{68}Ga-DOTATOC, ^{68}Ga-DOTATATE, and ^{68}Ga-DOTANOC have shown promise for neuroendocrine tumor imaging (*17–19*) and are used in clinical trials as well as under the local practice of pharmacy, particularly in Europe. Nevertheless, ^{68}Ga-PET imaging is not widely available because of the limited daily availability of [68]Ga (~50 mCi) and the lack of Food and Drug Administration–approved [68]Ge/^{68}Ga generators (*20*).

[18]F-fluoride presents several attractive properties for imaging (*21,22*) and is produced on a daily basis in large quantities in hundreds of cyclotrons in hospitals and radiopharmacies worldwide. Yet the challenges of labeling peptides with ^{18}F-fluoride are significant: the low chemical reactivity of ^{18}F-fluoride in water (*23*) and short half-life (109.8 min) challenge ^{18}F labeling of peptides that are generally soluble only in water or aqueous cosolvents. Hence, fluoride must be dried and reacted in dry solvents at high temperature to radiolabel a radioprosthetic that is then conjugated to the peptide in at least 1 additional step. Although such multistep ^{18}F-labeling reactions are commonplace (*24*), the relatively short half-life of ^{18}F-fluoride often impedes the clinical application of multistep reactions, particularly in terms of ensuring specific activity greater than 37 GBq/µmol (>1 Ci/µmol) (*25*). Given these challenges, an sstr2 ligand that is easily labeled with ^{18}F-fluoride in high yield and at high specific activity would facilitate sstr2 imaging by PET. Toward these ends, new ^{18}F-octreotate derivatives, such as ^{18}F-SiFA and Al-^{18}F-NOTA, have been labeled in 1 step and imaged with relative success (*26–28*).

Similarly, aryltrifluoroborate prosthetics, when conjugated to various peptides, allow 1-step aqueous radiofluorination in high yield and very high specific activity (*29–31*). Recently, we identified a new ammoniomethyl-BF$_3$ (AMBF$_3$) that undergoes facile [18]F-^{19}F isotope exchange. To test the efficacy of boron-based ^{18}F labeling, we conjugated AMBF$_3$ to octreotate by means of a simple chemical synthesis to obtain AMBF$_3$-TATE, which as a precursor is ^{18}F-labeled by isotope exchange (Compound **2,** Fig. 1). We report the radiosynthesis and preclinical evaluation of this new derivative.
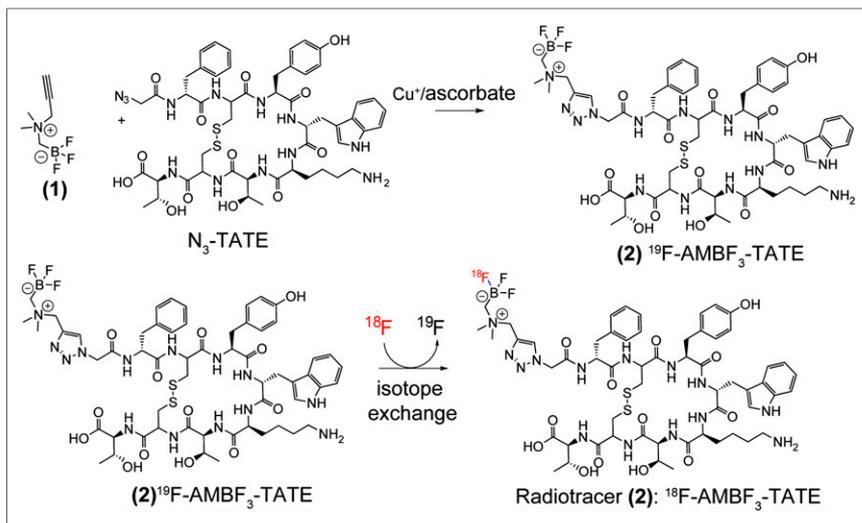
FIGURE 1. N$_3$-TATE is condensed with *N*-propargyl-*N,N*-dimethyl-ammoniomethyltrifluoroborate (**1**) to provide precursor AMBF$_3$-TATE (**2**). Precursor **2** is labeled by isotope exchange to provide isotopolog ^{18}F-**2** at high specific activity for tracer studies.

MATERIALS AND METHODS

Reagents and solvents were purchased from Advanced Chemtech, Sigma-Aldrich, Combi-Blocks, or Novabiochem. The AR42J cell line was purchased from ATCC. ^{18}F-fluoride Trap & Release Columns were purchased from ORTG Inc., and C18 Sep-Pak cartridges (1 cm^3, 50 mg) were obtained from Waters. An Endeavor 90 peptide synthesizer (Aapptec) was applied to synthesize the peptide. Electron-spray ionization low-resolution mass spectroscopy was performed on a Waters ZQ with a single quadrupole detector, attached to a Waters 2695 high-performance liquid chromatography (HPLC) column. All nuclear MR spectra were recorded at room temperature on a Bruker Avance 300 MHz spectrometer.

The following HPLC methods were used for purification and quality control. Method A: Agilent Eclipse XDB-C18 5-μm 9.2 × 250 mm semipreparative column; solvent A, 0.1% trifluoroacetic acid (TFA) water; solvent B, MeCN; 0–15 min, 20%–40% B; 15–20 min, 40%–20% B; flow rate, 4.5 mL/min; column temperature, 19°C–21°C. Method B: Agilent Eclipse XDB-C18 5-μm 9.2 × 250 mm semipreparative column; solvent A, 0.1% TFA water; solvent B, MeCN; 0–2 min, 5%–20% B; 2–5 min, 20%–30% B; 5–20 min, 30%–50%; 20–22 min, 50%–5% B; flow rate, 3 mL/min; column temperature, 19°C–21°C. Method C: Phenomenex Jupiter 10-μm C18 300-Å 4.6 × 250 mm analytic column; solvent A, 0.1% TFA water; solvent B, MeCN; 0–2 min, 5%–5% B; 2–7 min, 5%–20% B; 7–15 min, 20%–100%; 15–20 min, 100%–5% B; flow rate, 2 mL/min; column temperature, 19°C–21°C.

To synthesize the precursor for labeling, a suitable TATE was first synthesized as previously described (*32*) and converted to an azide derivative. The resin (Fmoc-Thr(tBu)-Wang) and growing chain were treated with 20% piperidine (1 × 5 min and 1 × 10 min) in *N,N*-dimethylformamide to remove the N$^\alpha$-Fmoc protecting group. The amino acids (3 equivalents [eq.] per coupling) Fmoc-Cys(Acm)-OH, Fmoc-Thr(tBu)-OH, Fmoc-Lys(Boc)-OH, Fmoc-D-Trp(Boc)-OH, Fmoc-Tyr(tBu)-OH, and Fmoc-D-Phe-OH were subsequently coupled in nuclear matrix protein with the standard in situ activating reagent *O*-benzotriazole-*N,N,N′,N′*-tetramethyl-uronium-hexafluoro-phosphate (HBTU) (3 eq.) in the presence of diisopropylethylamine (6 eq.). Thallium(III) trifluoroacetate (2 eq.) in *N,N*-dimethylformamide deprotected the cysteines and concomitantly induced disulfide formation. Bromoacetic acid (40 eq.) was preactivated with diisopropyl-carbodiimide (20 eq.) in dichloromethane for 10 min, filtered, and coupled to

the N terminus. NaN$_3$ (27.5 eq.) in dimethyl sulfoxide was added. The peptide was deprotected and simultaneously cleaved from the resin in 90:2.5:2.5:5 TFA:H$_2$O:triisopropylsilane:phenol for 4 h at room temperature. TATE-N$_3$ was purified by HPLC with a semipreparative column using method A to afford pure TATE-N$_3$ in quantities of about 10 mg. The calculated mass was 1,131.2, and the measured mass by electrospray ionization was 1,131.4. The purity of the peptide was greater than 99%. *N*-propargyl-*N,N*-dimethyl-ammoniomethyl-boronylpinacolate (alkynyl-AMB(pin)) was first synthesized by condensation of iodomethyl-boronylpinacolate and propargylamine as previously described (*33*). Briefly, a dry round-bottomed flask was charged with *N,N*-di-methylpropargylamine (98 μL, 1.0 mmol) and 2 mL of anhydrous diethyl ether under argon, to which iodomethyl-boronylpinacolate (165 μL, 0.9 mmol) was added dropwise at room temperature. On stirring, the solution became cloudy and the desired product was collected as a white precipitate that was filtered and washed with cold Et$_2$O and then dried under high vacuum to give a fluffy white powder in 95% yield. ^{1}H nuclear MR (300 MHz [Bruker], CD$_3$CN): δ 4.40 (d, 2H), 3.31 (s, 2H), 3.22 (s, 6H), 3.21 (t, 1H), 1.27 (s, 12H); electrospray ionization: calculated, 224.1; found, 224.1. *N*-propargyl-*N,N*-dimethyl-ammonio-methylboronylpinacolate (5.0 mg, 22.3 μmol) was converted to the trifluoroborate (alkynyl-AMBF$_3$) through the addition of KHF$_2$ (3 M, 30 μL in water), HCl (4 M, 30 μL in water), deionized water (20 μL), and *N,N*-dimethylformamide (60 μL), 45°C, 2 h, and then quenched by NH$_4$OH (concentration, 10 μL). The crude reaction was directly used for click conjugation to TATE azide without further purification: a mixture of TATE-azide (4.0 mg, 3.4 μmol), CuSO$_4$ (1.0 M, 5.0 μL), sodium ascorbate (1.0 M, 12.5 μL), and 5% NH$_4$OH (1:1 MeCN:H$_2$O, 50 μL) was added, and the mixture was heated to 45°C for 2 h. Purification was performed with method B to isolate 2.3 mg of AMBF$_3$-TATE. Purity was confirmed with liquid chromatography–mass spectrometry (calculated, 1,296.5; obtained, 1,296.4). The purified ^{19}F-AMBF$_3$-TATE was diluted in ethanol and portioned into aliquots of approximately 60 μg (50 nmol) for radiolabeling in kitlike fashion.

After successful synthesis, the activity of ^{19}F-AMBF$_3$-TATE was examined in vitro. Membranes from Chinese hamster ovary K1 cells transfected with sstr1, sstr2, sstr3, sstr5, and [^{125}I]-Tyr-somatostatin-14 were obtained from PerkinElmer. A standard filtration binding assay was performed in 96-well plates (MultiScreen; Millipore) to determine the binding affinities (inhibition constant, or K$_i$) of AMBF$_3$-TATE against different receptor subtypes. Briefly, membranes (0.25 μL/well) were incubated with the ^{125}I-labeled standard at a concentration of 0.05 nM for sstr2 or 0.2 nM for other subtypes. Increasing concentrations of AMBF$_3$-TATE were added to the wells in buffer (25 mM *N*-2-hydroxy-ethylpiperazine-*N*-2-ethanesulfonic acid, pH 7.4; 10 mM MgCl$_2$; 1 mM CaCl$_2$; and 0.5% bovine serum albumin). After incubation (37°C, 1 h), the wells were aspirated and washed 8 times with 50 mM ice-cold buffer (Tris-HCl, pH 7.4) over grade GF/B filters. The filters were removed and counted by a γ counter (Cobra II; Packard). A typical competition curve is shown in Figure 2 ($n = 3$). Data were fitted to a 1-site competition model (GraphPad Prism 6.1 software) to calculate K$_i$.

For ^{18}F labeling, AMBF$_3$-TATE (50 nmol) was resuspended in aqueous pyridazine-HCl buffer (~50 μL, pH 2) in a vial (polypropylene Falcon Tube; Corning) just before labeling. No-carrier-added ^{18}F-fluoride,
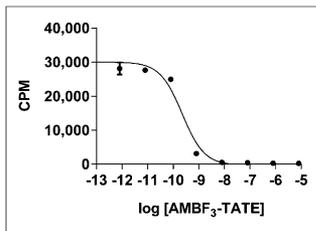
FIGURE 2. Representative example of competitive binding assay for ^{19}F-AMBF$_3$-TATE. y-axis shows counts bound. Assay was run with triplicate data points. CPM = counts per minute.

29.6–37 GBq (800–1,000 mCi), was obtained by bombardment of H$_2$^{18}O with 18-MeV protons, followed by trapping on an anion exchange resin (9 mg, quaternary ammonium, chloride form, prewashed with deionized water). The ^{18}F-fluoride was eluted with 70–100 μL of isotonic saline into the reaction vial containing AMBF$_3$-TATE. The vial was placed in a heating block set at 80°C for 20 min, whereupon the reaction was quenched by the injection of 2 mL of 5% NH$_4$OH in water. The reaction mixture was loaded onto a C18 light cartridge that was preconditioned by wetting with MeCN and washing with distilled water. Impurities (e.g., ^{18}F-fluoride, pyridazine) were removed by flushing with 2 mL of saline. Radiochemically pure ^{18}F-AMBF$_3$-TATE was released into a glass vial with 0.5 mL of 1:1 ethanol:saline to provide 7.4 GBq (200 mCi) of tracer. This solution was formulated in isotonic saline (5 mL). A small sample was removed for quality control analysis by HPLC with mass detection at 277 nm (Fig. 3). Radiochemically pure ^{18}F-AMBF$_3$-TATE, formulated in saline, was assayed for plasma stability. For this assay, 20 μL of ^{18}F-AMBF$_3$-TATE were added to mouse plasma (500 μL) and incubated at 37°C for 0, 60, and 120 min. After incubation at each time point, the reaction was quenched by adding 1 mL of MeCN to precipitate insoluble proteins from the solution. The quenched reactions were centrifuged to remove insoluble material. The supernatant was aspirated, filtered, and analyzed by HPLC using method C.

After labeling, imaging was undertaken. All animal studies were performed in accordance with the Canadian Council on Animal Care guidelines and were approved by the animal care committee of the University of British Columbia. Rat pancreatic adenocarcinoma cells (10^7 AR42J cells) were freshly expanded in a mixture of phosphate-buffered saline and Matrigel (Corning) and inoculated subcutaneously in female immunocompromised mice (NOD SCID [nonobese diabetic severe combined immunodeficient] IL2r-γ-null, bred in house). The tumors were grown for 2 wk until they reached 5–7 mm in diameter. While under 2% isoflurane anesthesia, the mice were injected via the tail vein with 0.37–0.74 MBq (10–20 μCi, 4–8 pmol) of ^{18}F-AMBF$_3$-TATE ($n = 5$). To demonstrate the specificity of in vivo uptake in receptor-positive tissues, 100 μg of $^{69/71}$Ga-DOTATATE were preinjected 15 min before ^{18}F-AMBF$_3$-TATE injection as a blocking control cohort ($n = 4$). Sixty minutes after injection, the mice were anesthetized with isoflurane and euthanized by carbon dioxide. The organs were harvested, rinsed with saline, blotted dry, and collected in previously weighed tubes. The tubes containing the organs were counted in a Cobra-II γ counter. The tissue weight and associated count per minute were used to calculate the percentage injected dose per gram of tissue (%ID/g). Images were acquired using a multimodality PET/CT system (Inveon; Siemens). Approximately 3.7 MBq (100 μCi, ~40 pmol) of radiotracer were injected in the caudal lateral tail vein of tumor-bearing mice. Sixty minutes after radiotracer injection, the animals were anesthetized with isoflurane inhalation and a baseline low-dose CT scan was obtained for localization and attenuation correction, followed by a static PET scan acquired for 10 min. The mice were kept warm by a heated pad on the scanner bed during acquisition. $^{69/71}$Ga-DOTATATE (100 μg per mouse) was preinjected as a blocking agent. The images were reconstructed by an iterative reconstruction algorithm (3-dimensional ordered-subsets expectation maximization/maximum a posteriori) using the Inveon Acquisition Workplace Software (Siemens), applying normalization, dead time, random, and attenuation corrections. Uptake into tumor and tissues of interest was determined by regions of interest, and %ID/g was calculated (assuming a tissue density of 1.0 g/cm^3). The mean %ID/g was calculated from a region of interest that matched the tumor contours on CT. The peak %ID/g was calculated from the hottest 2 × 2 voxel cluster within the tumor. In 1 animal, a dynamic scan was acquired in list mode for 60 min under continuous isoflurane inhalation, starting concurrently with radiotracer injection. Imaging data from this mouse were not combined with the results of static imaging and were used to obtain the tissue time–activity curves reported in Figure 4.
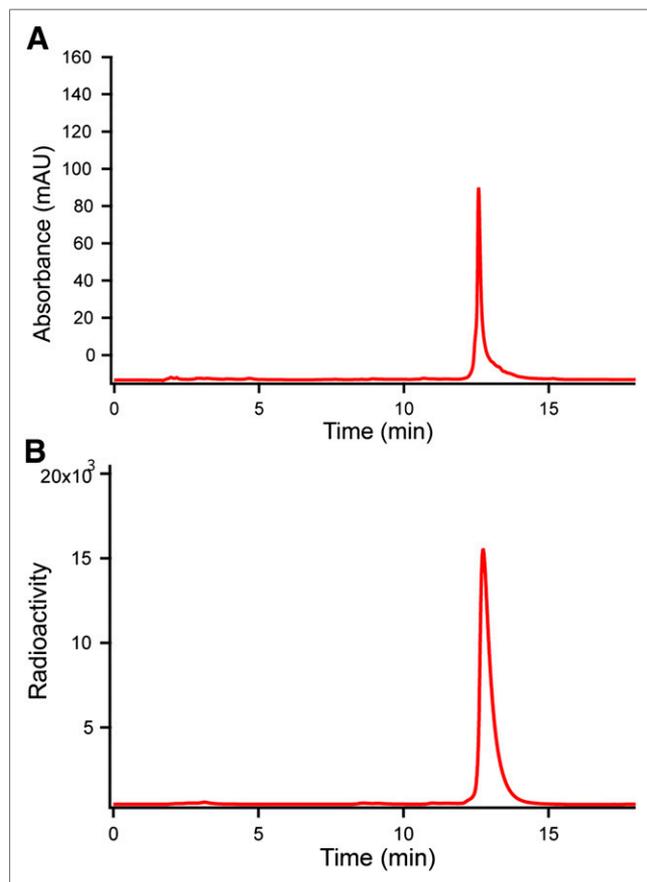

FIGURE 3. HPLC traces of Sep-Pak–purified ^{18}F-AMBF$_3$-TATE. (A) Ultraviolet trace measured at 277 nm. (B) Radioactivity trace. AU = arbitrary units.
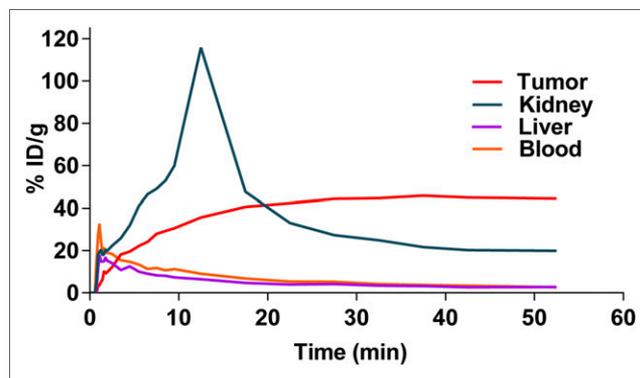

FIGURE 4. Time–activity curves indicating blood, liver, and kidney clearance and peak tumor uptake (from hottest voxel cluster in tumor from a single mouse).
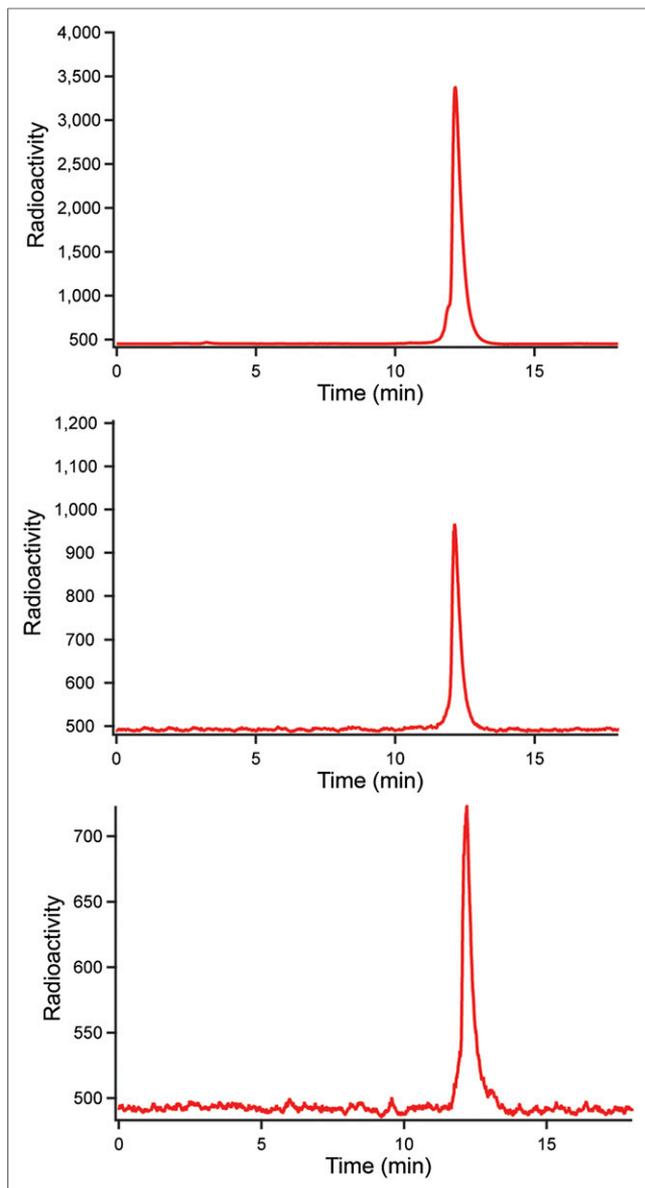
FIGURE 5. Plasma stability assay of ^{18}F-AMBF$_3$-TATE; radiotraces are shown for 0, 60, and 120 min.

RESULTS

In Vitro Affinity

The K$_i$ of AMBF$_3$-TATE using human sstr2 receptors expressed on Chinese hamster ovary membranes was 0.13 ± 0.03 nM. Using identical assay conditions and the same lot of membranes, the K$_i$ for gallium-DOTATATE was 0.7 ± 0.2 nM. A representative competitive binding assay curve is shown in Figure 2. No significant displacement of binding to sstr1 was observed. The inhibition constants for sstr3 and sstr5 were 28.4 ± 8.6 nM and 11.6 ± 2.8 nM, respectively.

Radiosynthesis

Starting with 29.6–37 GBq of no-carrier-added ^{18}F-fluoride (800–1,000 mCi), approximately 7.4 GBq of ^{18}F-AMBF$_3$-TATE were obtained within 25 min (24% ± 4%, n = 5) and reinjected into HPLC for quality analysis (Fig. 3), which showed a single peak in both radioactive and ultraviolet modes. Because approximately
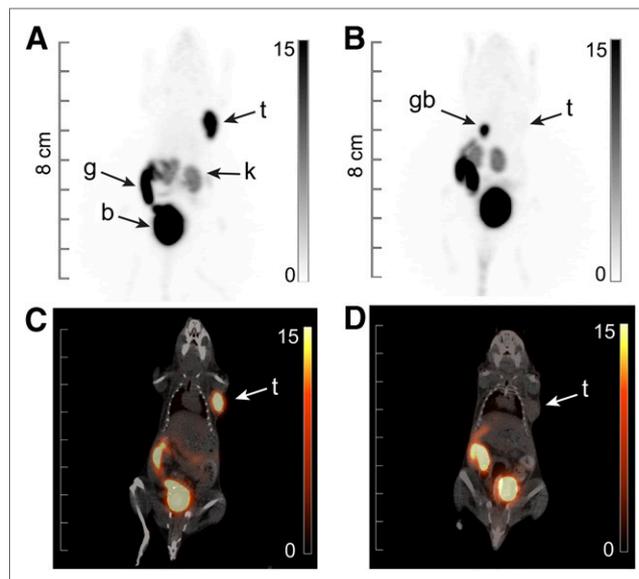

FIGURE 6. ^{18}F-AMBF$_3$-TATE PET images of AR42J tumor–bearing mice at 60 min after injection: unblocked (A and C) and blocked (B and D). Upper panels are maximum-intensity-projection images; bottom panels are corresponding fused coronal images. Color bars are calibrated in %ID/g with no background subtracted. Tracer specifically accumulated into tumor (t), whereas remainder rapidly cleared via kidneys (k) to bladder (b). Some gut (g) and gallbladder (gb) accumulation occurred because of rapid hepatobiliary excretion.

7.4 GBq (~200 mCi) of **2** were obtained starting with 50 nmol of precursor, the specific activity was 148 GBq/μmol (3 Ci/μmol), with a radiochemical yield of 20%–25% (not corrected for decay). To validate this calculation, a standard curve showed that the

TABLE 1
Biodistribution of ^{18}F-AMBF$_3$-TATE (%ID/g)

| Tissues	Unblocked		Blocked	
	Average	SD	Average	SD
Blood	0.40	0.31	0.32	0.15
Plasma	0.72	0.71	0.92	0.16
Uterus	0.26	0.05	0.51	0.11
Large intestine	2.28	2.64	4.27	6.20
Small intestine	3.23	1.58	1.82	1.70
Spleen	0.42	0.19	0.31	0.11
Liver	0.39	0.05	0.41	0.14
Pancreas	2.81	1.49	0.20	0.01
Adrenal glands	0.54	0.18	0.28	0.07
Kidney	4.90	1.54	4.50	3.54
Lungs	1.85	0.83	0.79	0.26
Heart	0.17	0.05	0.88	1.12
Tumor	10.11	1.67	0.32	0.21
Muscle	0.11	0.03	0.11	0.09
Bone	0.46	0.17	0.54	0.36
Brain	0.03	0.01	0.22	0.33
Tail	0.28	0.06	0.38	0.09
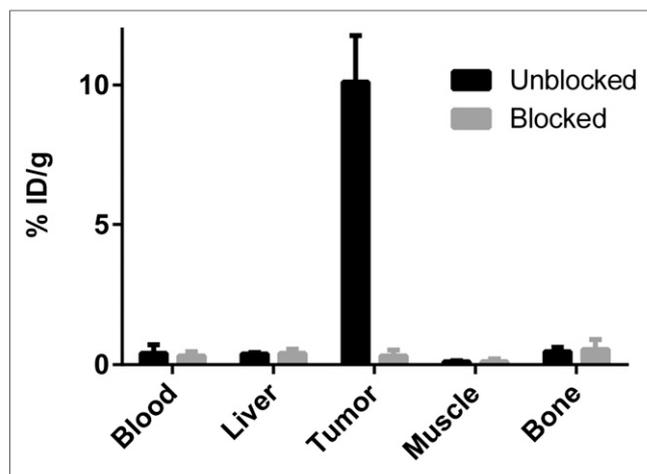
FIGURE 7. Selected organs from biodistribution of ^{18}F-AMBF$_3$-TATE at 60 min after injection in AR42J-bearing mice, showing high receptor-mediated uptake in tumors compared with normal tissues.

specific activity was more than 111 GBq/μmol (>3 Ci/μmol). ^{18}F-AMBF$_3$-TATE was incubated in mouse plasma for 120 min with no detectable decomposition (Fig. 5).

PET/CT Imaging

Uptake in the AR42J tumors was intense and clearly specific as evidenced by the lack of uptake in the tumors of mice receiving unlabeled competitor (Fig. 6). The average of the tumor uptake based on the whole tumor region of interest was 10.2 ± 2.1 %ID/g. The average of the peak tumor uptake based on the hottest voxel cluster was 23.6 ± 3.0 %ID/g. In contrast, the average uptake in the liver, blood pool, and muscle was 0.83 ± 0.16, 0.47 ± 0.12, and 0.09 ± 0.03 %ID/g, respectively. Excretion was predominantly renal, with significant clearance to the bladder and low kidney retention. Some hepatobiliary tract excretion was notably rapid, leading to high tumor-to-liver ratios. Bone uptake was undetectable, and there was low background activity in blood and muscle, resulting in high-contrast images.

Pharmacokinetics (Time–Activity Curve Analysis)

Time–activity curves of uptake in tumor and other tissues from a tumor-bearing mouse are presented in Figure 4. Time-dependent tumor uptake increased to a peak voxel cluster value of approximately 40 %ID/g in a mouse with a fairly large tumor. Uptake in nontarget tissues rapidly declined after reaching the peak value at a time point soon after intravenous administration.

Biodistribution Studies

The ex vivo biodistribution data of ^{18}F-AMBF$_3$-TATE at 1 h (Table 1) corroborate the scanning data. The relative uptake values in various tissues are shown in Figure 7. Uptake in AR42J xenograft tumors in the unblocked mice was 10.11 ± 1.67 %ID/g. As expected, excess competitor caused a substantial reduction in tumor uptake: 0.32 ± 0.21 %ID/g. Hence, blocking efficiency was 97%. Uptake values in blood and muscle were low: 0.40 ± 0.31 %ID/g and 0.11 ± 0.03 %ID/g, respectively, which gave high tumor-to-blood and tumor-to-muscle ratios of 25.1 ± 1.0 and 89.0 ± 3.1, respectively. Bone uptake was negligible (0.46 ± 0.17 %ID/g), indicating no in vivo defluorination.

DISCUSSION

Isotope exchange on the organotrifluoroborate prosthetic greatly simplified labeling on several accounts. First, only submilligram quantities of precursor were needed for labeling. Second, no time-consuming azeotropic fluoride drying was required, because no-carrier-added ^{18}F-fluoride was eluted in isotonic saline and used directly for an aqueous labeling reaction. Third, labeling was rapid (~20 min) and provided for high specific activity. Fourth, because the precursor is chemically identical to the product, time-consuming HPLC purification was obviated in favor of a simple C18 Sep-Pak elution to remove free fluoride. Besides the methodologic simplicity, the yields provide multiple human doses in a single run. In light of

TABLE 2
Comparison of Some Octreotide and Octreotate Derivatives

Ligand	Synthesis time (min)	Specific activity (GBq/μmol)	HPLC purification	Tumor type	Tumor %ID/g
^{111}In-DTPA-pentetreotide (37)	>60	44.2	No	AR42J	0.99*
^{99m}Tc-depreotide (37)	20	37	No	CA20948	4.81†
^{111}In-DOTA-TATE (8)	>60	15.9	No	AR42J	4.12*
^{99m}Tc-EDDA/HYNIC-TATE (8)	20	60	No	AR42J	5.01
^{64}Cu-TE1A1P-Y3-TATE (13)	>60	48	No	AR42J	5.11
^{18}F-FETE-PEG-TOCA (16)	90	5.9	Yes	AR42J	5.14
^{18}F-FET-bAG-TOCA (16)	90	3.9	Yes	AR42J	8.23
^{18}F-FET-bAG-[W-c-K] (16)	90	12.3	Yes	AR42J	0.11
^{18}F-AlF-NOTA-OC (28)	45	36.1	No	AR42J	6.43
^{18}F-SiFA-Tyr^3-OC (26)	<30	29–56	No	AR42J	7.73
^{68}Ga-DOTA-TATE (19)	45	Not given	No	AR42J	2.75
^{18}F-AMBF$_3$-TATE (this work)	<30	111	No	AR42J	10.11

*4-h time point.
†90-min time point.

improvements in cyclotron output to provide multiple-curie levels of ^{18}F-fluoride (*34*), this methodology is readily applicable to existing production facilities. Moreover, the simplicity of the process should be easily amenable to automation and microfluidic flow technologies.

Whereas good radiosynthetic attributes are a prerequisite for use, the real value of a given tracer ultimately lies in the in vivo image data and corroborating biodistribution data. There is an extensive body of literature, which cannot be fully reviewed here, detailing the labeling and imaging of various TATE analogs by SPECT or PET. A brief comparison of the representative radiolabeled TATE derivatives is featured in Table 2. Comparison of receptor binding affinities is difficult because many authors report an inhibitory concentration of 50%, which is dependent on assay conditions. Among the published TATE-based radiotracers, gallium-DOTATATE has the highest affinity for sstr2 reported to date. Under identical conditions, ^{18}F-AMBF$_3$-TATE showed higher affinity than gallium-DOTATATE. This finding was both unanticipated and significant. The sensitivity of somatostatin analogs, either agonists or antagonists, to substitutions at the N terminus and to the radiometal is well documented (*35,36*). Here, the octreotate was modified with the AMBF$_3$ prosthetic via copper-catalyzed click conjugation; although we expected a decrease in the binding affinity to the sstr2, we instead observed a more than 5-fold higher binding affinity than for ^{68}Ga-DOTATATE as assayed under identical conditions. The inhibition constants to sstr3 and sstr5 also appeared to be lower than the values published for Ga-DOTATATE, suggesting that other zwitterionic moieties at the N terminus may improve affinity.

On the basis of PET/CT imaging, ^{18}F-AMBF$_3$-TATE exhibited low background activity in nontarget tissues and high receptor-mediated uptake in a preclinical murine model of sstr2-positive cancer. Corroborating the in vivo imaging data, ex vivo biodistribution verified the high tumor uptake values. Although liver uptake of radiometallated octreotides typically is low, this is not always the case for ^{18}F-labeled octreotides. Liver uptake, and in particular nonspecific uptake, is often observed and may preclude clinical detection of liver metastasis. Interestingly, the liver uptake of ^{18}F-AMBF$_3$-TATE was low, resulting in a higher tumor-to-liver ratio (26.21 ± 0.79 1 h after injection) than has been reported for other ^{18}F-labeled TATE analogs (0.25–5.0 2 h after injection) (*16,26*).

A plasma stability assay (37°C) showed negligible decomposition of ^{18}F-AMBF$_3$-TATE after 120 min. Consistent with this finding, minimal bone uptake was observed in both PET/CT and biodistribution, resulting in a high tumor-to-bone ratio of up to 21.3 ± 3.6. This low, nonspecific bone uptake is particularly encouraging for the detection of bone metastasis. Moreover, this result highlights the general stability of such alkyltrifluoroborate radioprosthetics, an observation that should augur well for the development of other peptide tracers based on the same zwitterionic ammoniomethyl-BF$_3$.

CONCLUSION

We report a high-affinity octreotate–organotrifluoroborate conjugate that was radiolabeled with ^{18}F in high yield and high specific activity via a facile isotope exchange reaction using minute quantities of precursor peptide, without HPLC purification. This methodology provides for rapid, multidose tracer production in a single run that should be amenable to automation. In addition to radiosynthetic ease, the biologic evaluation of ^{18}F-AMBF$_3$-TATE indicated that this tracer provides good stability, optimal pharmacokinetics, excellent binding affinity, and high tumor–to–nontarget-tissue ratios for in vivo imaging.

REFERENCES

1. Kwekkeboom DJ, de Herder WW, van Eijck CH, et al. Peptide receptor radio-nuclide therapy in patients with gastroenteropancreatic neuroendocrine tumors. *Semin Nucl Med.* 2010;40:78–88.
2. Breeman WAP, de Jong M, Kwekkeboom DJ, et al. Somatostatin receptor-mediated imaging and therapy: basic science, current knowledge, limitations and future perspectives. *Eur J Nucl Med.* 2001;28:1421–1429.
3. Ginj M, Schmitt JS, Chen JH, et al. Design, synthesis, and biological evaluation of somatostatin-based radiopeptides. *Chem Biol.* 2006;13:1081–1090.
4. Antunes P, Ginj M, Walter MA, et al. Influence of different spacers on the biological profile of a DOTA-somatostatin analogue. *Bioconjug Chem.* 2007;18:84–92.
5. Kwekkeboom DJ, Kam BL, van Essen M, et al. Somatostatin receptor-based imaging and therapy of gastroenteropancreatic neuroendocrine tumors. *Endocr Relat Cancer.* 2010;17:R53–R73.
6. Krausz Y, Keidar Z, Kogan I, et al. SPECT/CT hybrid imaging with In-111-pentetreotide in assessment of neuroendocrine tumours. *Clin Endocrinol (Oxf).* 2003;59:565–573.
7. Buchmann I, Henze M, Engelbrecht S, et al. Comparison of Ga-68-DOTATOC PET and In-111-DTPAOC (Octreoscan) SPECT in patients with neuroendocrine tumours. *Eur J Nucl Med Mol Imaging.* 2007;34:1617–1626.
8. Storch D, Behe M, Walter MA, et al. Evaluation of [^{99m}Tc/EDDA/HYNIC0] octreotide derivatives compared with [^{111}In-DOTA0,Tyr3, Thr8]octreotide and [^{111}In-DTPA0]octreotide: does tumor or pancreas uptake correlate with the rate of internalization? *J Nucl Med.* 2005;46:1561–1569.
9. Virgolini I, Leimer M, Handmaker H, et al. Somatostatin receptor subtype specificity and in vivo binding of a novel tumor tracer, ^{99m}Tc-P829. *Cancer Res.* 1998;58:1850–1859.
10. Gabriel M, Decristoforo C, Donnemiller E, et al. An intrapatient comparison of ^{99m}Tc-EDDA/HYNIC-TOC with ^{111}In-DTPA-octreotide for diagnosis of somatostatin receptor-expressing tumors. *J Nucl Med.* 2003;44:708–716.
11. Sprague JE, Peng YJ, Sun XK, et al. Preparation and biological evaluation of copper-64-labeled tyr3-octreotate using a cross-bridged macrocyclic chelator. *Clin Cancer Res.* 2004;10:8674–8682.
12. Gabriel M, Decristoforo C, Kendler D, et al. Ga-68-DOTA-Tyr3-octreotide PET in neuroendocrine tumors: comparison with somatostatin receptor scintigraphy and CT. *J Nucl Med.* 2007;48:508–518.
13. Guo Y, Ferdani R, Anderson CJ. Preparation and biological evaluation of Cu-64 labeled tyr3-octreotate using a phosphonic acid-based cross-bridged macrocyclic chelator. *Bioconjug Chem.* 2012;23:1470–1477.
14. Wester HJ, Schottelius M, Scheidhauer K, et al. PET imaging of somatostatin receptors: design, synthesis and preclinical evaluation of a novel F-18-labelled, carbohydrated analogue of octreotide. *Eur J Nucl Med Mol Imaging.* 2003;30:117–122.
15. Poethko T, Schottelius M, Thumshim G, et al. Two-step methodology for high-yield routine radiohalogenation of peptides: ^{18}F-labeled RGD and octreotide analogs. *J Nucl Med.* 2004;45:892–902.
16. Leyton J, Iddon L, Perumal M, et al. Targeting somatostatin receptors: preclinical evaluation of novel F-18-fluoroethyltriazole-tyr3-octreotate analogs for PET. *J Nucl Med.* 2011;52:1441–1448.
17. Henze M, Schuhmacher J, Hipp P, et al. PET imaging of somatostatin receptors using [^{68}GA]DOTA-D-Phe1-Tyr3-octreotide: first results in patients with meningiomas. *J Nucl Med.* 2001;42:1053–1056.

18. Kayani I, Conry BG, Groves AM, et al. A comparison of Ga-68-DOTATATE and F-18-FDG PET/CT in pulmonary neuroendocrine tumors. *J Nucl Med.* 2009;50:1927–1932.

19. Poeppel TD, Binse I, Petersenn S, et al. Ga-68-DOTATOC versus Ga-68-DOTATATE PET/CT in functional imaging of neuroendocrine tumors. *J Nucl Med.* 2011;52:1864–1870.

20. Banerjee SR, Pomper MG. Clinical applications of gallium-68. *Appl Radiat Isot.* 2013;76:2–13.

21. Laforest R, Liu X. Image quality with non-standard nuclides in PET. *Q J Nucl Med Mol Imaging.* 2008;52:151–158.

22. Kemerink GJ, Visser MGW, Franssen R, et al. Effect of the positron range of F-18, Ga-68 and I-124 on PET/CT in lung-equivalent materials. *Eur J Nucl Med Mol Imaging.* 2011;38:940–948.

23. Zhan C-G, Dixon DA. Hydration of the fluoride anion: structures and absolute hydration free energy from first-principles electronic structure calculations. *J Phys Chem A.* 2004;108:2020–2029.

24. Chin FT, Shen B, Liu SL, et al. First experience with clinical-grade F-18 FPP (RGD)(2): an automated multi-step radiosynthesis for clinical PET studies. *Mol Imaging Biol.* 2012;14:88–95.

25. Cai H, Conti PS. RGD-based PET tracers for imaging receptor integrin alpha$_v$beta$_3$ expression. *J Labelled Comp Radiopharm.* 2013;56:264–279.

26. Wängler C, Waser B, Alke A, et al. One-step F-18-labeling of carbohydrate-conjugated octreotate-derivatives containing a silicon-fluoride-acceptor (SiFA): in vitro and in vivo evaluation as tumor imaging agents for positron emission tomography (PET). *Bioconjug Chem.* 2010;21:2289–2296.

27. Laverman P, D'Souza CA, Eek A, et al. Optimized labeling of NOTA-conjugated octreotide with F-18. *Tumour Biol.* 2012;33:427–434.

28. Laverman P, McBride WJ, Sharkey RM, et al. A novel facile method of labeling octreotide with F-18-fluorine. *J Nucl Med.* 2010;51:454–461.

29. Liu Z, Li Y, Lozada J, et al. Rapid, one-step, high yielding ^{18}F-labeling of an aryltrifluoroborate bioconjugate by isotope exchange at very high specific activity. *J Labelled Comp Radiopharm.* 2012;14:491–497.

30. Liu Z, Li Y, Lozada J, et al. Kit-like ^{18}F-labeling of RGD-^{19}F-aryltrifluroborate in high yield and at extraordinarily high specific activity with preliminary in vivo tumor imaging. *Nucl Med Biol.* 2013;40:841–849.

31. Liu Z, Li Y, Lozada J, et al. Stoichiometric leverage: rapid ^{18}F-aryltrifluoroborate radiosynthesis at high specific activity for click conjugation. *Angew Chem Int Ed.* 2013;52:2305–2307.

32. Lewis JS, Srinivasan A, Schmidt MA, Anderson CJ. In vitro and in vivo evaluation of Cu-64-TETA-Tyr^3-octreotate: a new somatostatin analog with improved target tissue uptake. *Nucl Med Biol.* 1999;26:267–273.

33. Matteson DS, Majumdar D. Iodomethaneboronic esters and aminomethane boronic esters. *J Organomet Chem.* 1979;170:259–264.

34. Eberl S, Eriksson T, Svedberg O, et al. High beam current operation of a PETtrace™ cyclotron for [18]F$^-$ production. *Appl Radiat Isot.* 2012;70:922–930.

35. Fani M, Braun F, Waser B, et al. Unexpected sensitivity of sst2 antagonists to N-terminal radiometal modifications. *J Nucl Med.* 2012;53:1481–1489.

36. Reubi JC, Schar JC, Waser B, et al. Affinity profiles for human somatostatin receptor subtypes SST1-SST5 of somatostatin radiotracers selected for scintigraphic and radiotherapeutic use. *Eur J Nucl Med.* 2000;27:273–282.

37. Vallabhajosula S, Moyer BR, Lister-James J, et al. Preclinical evaluation of technetium-99m-labeled somatostatin receptor-binding peptides. *J Nucl Med.* 1996;37:1016–1022.